

1 Scaling of maximum probability density functions of velocity and temperature
2 increments in turbulent systems

Y.X. Huang (黄永祥),^{1,2, a)} F. G. Schmitt,^{3, 4, 5, b)} Q. Zhou (周全),^{1,2} X. Qiu (邱翔),⁶
 X.D. Shang (尚晓东),⁷ Z.M. Lu (卢志明),^{1,2} and Y.L. Liu (刘宇陆)¹

¹⁾*Shanghai Institute of Applied Mathematics and Mechanics,
 Shanghai Key Laboratory of Mechanics in Energy and Environment Engineering,
 Shanghai University, Shanghai 200072, China*

²⁾*Modern Mechanics Division, E-Institutes of Shanghai Universities,
 Shanghai University, Shanghai 200072, China*

³⁾*Université Lille Nord de France, F-59000 Lille, France*

⁴⁾*USTL, LOG, F-62930 Wimereux, France*

⁵⁾*CNRS, UMR 8187, F-62930 Wimereux, France*

⁶⁾*School of Science, Shanghai Institute of Technology, 200235, Shanghai,
 China*

⁷⁾*State Key Laboratory of Tropical Oceanography, South China Sea
 Institute of Oceanology, Chinese Academy of Sciences, Guangzhou 510301,
 China*

(Dated: 20 January 2014)

In this paper, we introduce a new way to estimate the scaling parameter of a self-similar process by considering the maximum probability density function (pdf) of its increments. We prove this for H -self-similar processes in general and experimentally investigate it for turbulent velocity and temperature increments. We consider turbulent velocity database from an experimental homogeneous and nearly isotropic turbulent channel flow, and temperature data set obtained near the sidewall of a Rayleigh-Bénard convection cell, where the turbulent flow is driven by buoyancy. For the former database, it is found that the maximum value of increment pdf $p_{\max}(\tau)$ is in a good agreement with lognormal distribution. We also obtain a scaling exponent $\alpha \simeq 0.37$, which is consistent with the scaling exponent for the first-order structure function reported in other studies. For the latter one, we obtain a scaling exponent $\alpha_\theta \simeq 0.33$. This index value is consistent with the Kolmogorov-Obukhov-Corrsin scaling for passive scalar turbulence, but different from the scaling exponent of the first-order structure function that is found to be $\zeta_\theta(1) \simeq 0.19$, which is in favor of Bolgiano-Obukhov scaling. A possible explanation for these results is also given.

PACS numbers: 94.05.Lk, 05.45.Tp, 47.27.Gs

19

^{a)}Electronic mail: yongxianghuang@gmail.com

^{b)}Electronic mail: francois.schmitt@univ-lille1.fr

I. INTRODUCTION

Since Kolmogorov's 1941 (K41) milestone work, the invariant properties of small-scale structures have been widely investigated during the last four decades.¹⁻⁵ The invariant properties are characterized by a series of scaling exponents $\zeta(q)$, which is traditionally extracted by the classical structure function (SF) analysis $S_q(\ell) = \langle \Delta u_\ell(r)^q \rangle \sim \ell^{\zeta(q)}$ that has been documented very well for turbulent velocity fields.^{2-4,6} Here, $\Delta u_\ell(r) = u(\ell + r) - u(r)$ is the velocity increment.

A key problem of turbulence is the search of universal probability density function (pdf) of turbulent velocity.^{3,7} The pdf of turbulent velocity or velocity increments has been studied by several authors.^{2,8-13} Several models of velocity increment have been proposed to characterize its pdf tail. For example, Anselmetti *et al.*² proposed an exponential fitting to extrapolate the pdf tail of velocity increments with separation scales in inertial range, which is also advocated in Ref. 8. Ching⁹ proposed a stretched exponential pdf of temperature increments for Rayleigh-Bénard convection (RBC) system. Later, it has been applied in turbulent velocity by Kailasnath, Sreenivasan, and Stolovitzky¹⁰.

In this paper, we investigate another aspect of the pdf scaling of increments of scaling time series, e.g. fractional Brownian motion (fBm), turbulent velocity, and temperature. We find a pdf scaling

$$p_{\max}(\tau) \sim \tau^{-\alpha} \quad (1)$$

for the maximum pdf of the increment Δu_τ . This pdf scaling can be obtained analytically for the fBm processes and more generally for H -self-similar processes, in which only one parameter Hurst number H is required to describe the processes, and we find in this case $\alpha = H$. For the fBm case, the pdf scaling is validated by numerical simulations. We hence postulate that the pdf scaling also holds for multifractal processes, such as turbulent velocity, temperature fluctuations in RBC system, etc. To our knowledge, the method we proposed here is the first method to extract scaling exponents on the probability space rather than on the statistical moments space, as usually done.

This paper is organized as following. In section II, we derive analytically a pdf scaling of increments for fractional Brownian motion processes and more generally for H -self-similar processes. In section III, we investigate the pdf scaling of velocity from turbulent channel flow and temperature from turbulent Rayleigh-Bénard convection system, respectively. We

50 finally present our discussions and draw the main conclusion in section IV.

51 II. FRACTIONAL BROWNIAN MOTION AND H -SELF-SIMILAR 52 PROCESSES

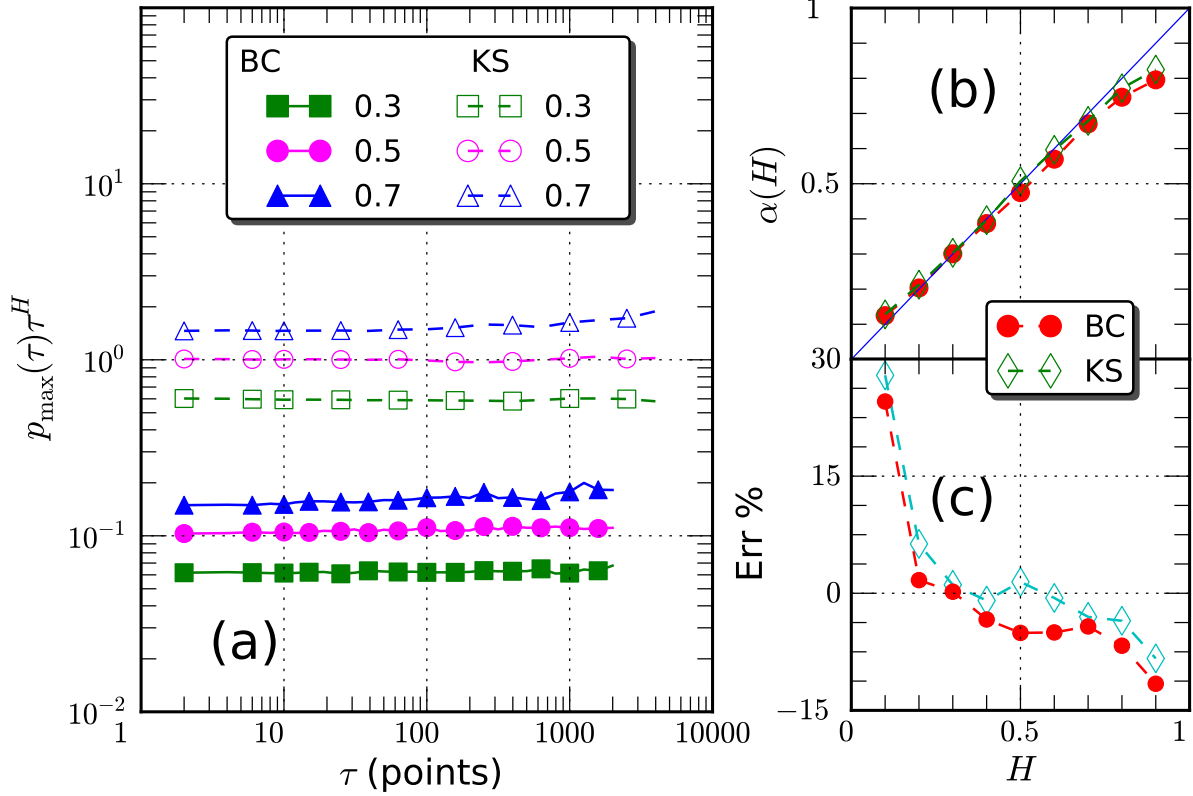


FIG. 1. (a) Compensated $p_{\max}(\tau)\tau^H$ estimated from fBm simulation with various Hurst numbers H by using box-counting method (denoted as BC) and a kernel smoothing method with Gaussian kernel (denoted as KS), (b) the corresponding scaling exponents $\alpha(H)$, where the theoretical value is illustrated by a solid line, and (c) the relative error $(\alpha - H)/H$ between given and estimated Hurst number. The scaling exponent is estimated on the range $10 < \tau < 1000$ data points by using a least square fitting algorithm.

53 A. Fractional Brownian motion

54 FBM is a continuous-time random process proposed by Kolmogorov¹⁴ in the 1940s and
55 Yaglom¹⁵ and later named ‘fractional Brownian motion’ by Mandelbrot¹⁶. It consists in a

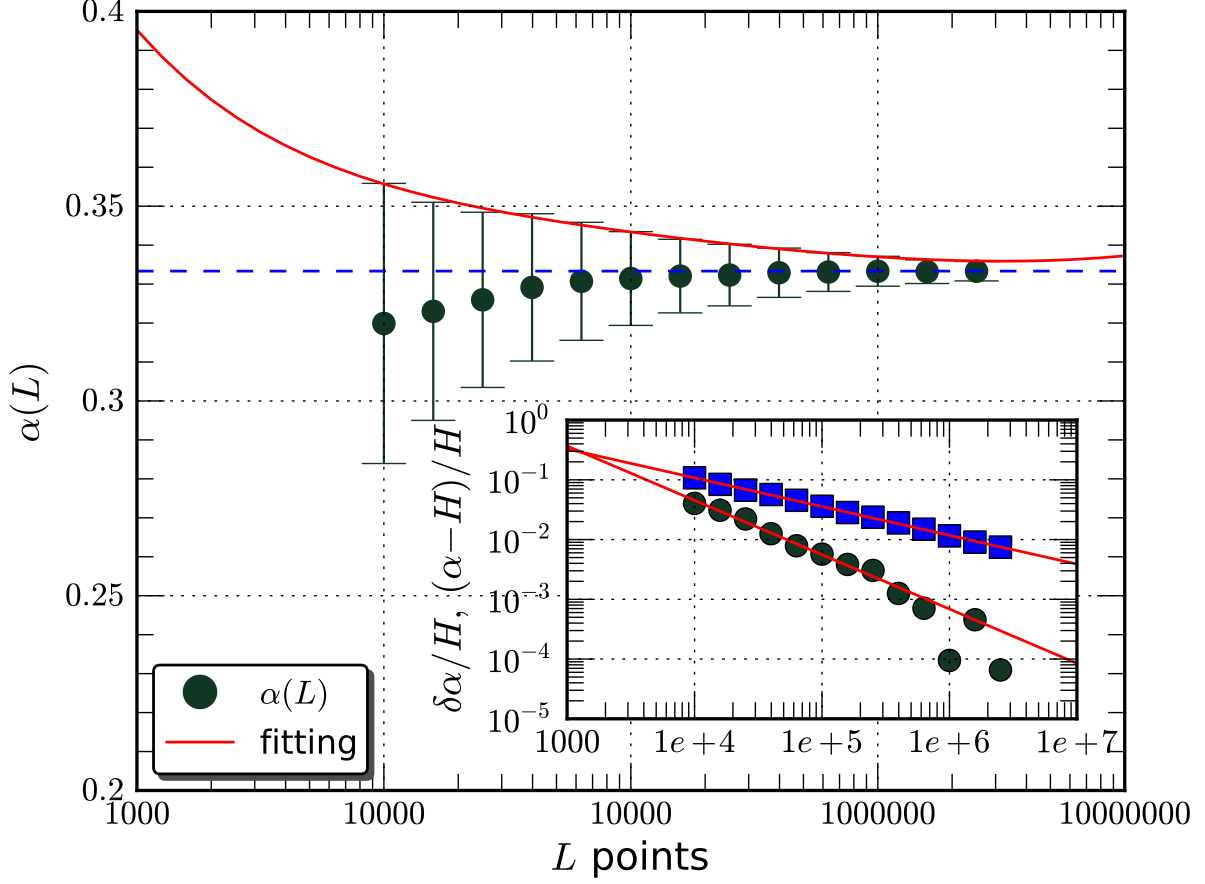


FIG. 2. The length dependent $\alpha(L)$ (\circ) for the Hurst number $H = 1/3$ with 1000 realizations (using box-counting method). The horizontal dashed line illustrates the given Hurst number $H = 1/3$. The solid line is the fitting of the errorbar (standard deviation of $\alpha(L)$). The inset shows the corresponding relative error $Er(L) = (H - \alpha(L))/H$ (\circ) and errorbar $\delta\alpha(L)/H$ (\square), in which the solid line is the power law fitting $Er(L) \sim L^{-\xi}$ and $\delta\alpha(L) \sim L^{-\gamma}$ with scaling exponents $\xi \simeq 0.91$ and $\gamma \simeq 0.49$ respectively.

fractional integration of a white Gaussian process and is therefore a generalization of Brownian motion, which consists simply in a standard integration of a white Gaussian process. Because it presents deep connections with the concepts of self-similarity, fractal, long-range dependence or $1/f$ -process, it quickly became a major tool for various fields where such concepts are relevant, such as in geophysics, hydrology, turbulence, economics, communications, etc.^{16–24} Below we consider it as an analytical model for monofractal processes to obtain the pdf scaling analytically.

An autocorrelation function of fBm's increments $Y_\tau(t) = x(t + \tau) - x(t)$ is known to be

the following

$$R_\tau(\ell) = \frac{1}{2}\{(\tau + \ell)^{2H} + |\tau - \ell|^{2H} - \ell^{2H}\} \quad (2)$$

where $\ell \geq 0$ is the time delay, τ is the separation scale, and H is Hurst number.²³ Thus the standard deviation $\sigma(Y_\tau)$ of the increment Y_τ scales as

$$\sigma(Y_\tau) = R_\tau(0)^{1/2} = \tau^H \quad (3)$$

Y_τ is also known to have a Gaussian distribution,^{16,23} which reads as

$$p(Y_\tau) = \frac{1}{\sigma(Y_\tau)\sqrt{2\pi}} \exp\left(-\frac{Y_\tau^2}{2\sigma(Y_\tau)^2}\right) \quad (4)$$

We thus have a power law relation when $Y_\tau = 0$

$$p_{\max}(\tau) = p(Y_\tau)|_{Y_\tau=0} = \frac{1}{\sigma(Y_\tau)\sqrt{2\pi}} = \frac{1}{\sqrt{2\pi}}\tau^{-\alpha(H)} \quad (5)$$

where $\alpha(H) = H$.

In order to numerically check this, we perform a wavelet based algorithm to simulate the fBm process.²⁵ We synthesize a segment of length 10^6 data points for each value of Hurst number H from 0.1 to 0.9 by using db2 wavelet. The pdfs are estimated as follows. We first normalize x by its own standard deviation σ . The empirical pdf is then estimated by using box-counting method on several discrete bins with width dh

$$p(Y) = \frac{N_i}{N dh} \quad (6)$$

in which N_i is the number of events in the i th bin, N is the total length of the data. We find that the empirical pdf $p(Y_\tau)$, the maxima pdf $p_{\max}(\tau) = \max_{Y_\tau} \{p(Y_\tau|\tau)\}$, and the corresponding scaling exponents $\alpha(H)$ are almost independent of the range of bin width dh . Another way to estimate the pdf is a kernel smoothing method.²⁶ In this study, a Gaussian kernel is chosen. Figure 1 (a) shows the estimated $p_{\max}(\tau)\tau^H$ for various Hurst numbers H . For both methods, a clear plateau is observed, indicating power law behavior as expected for all Hurst numbers. We estimate the scaling exponents on the range $10 < \tau < 1000$ data points by a least square fitting algorithm. The corresponding scaling exponents $\alpha(H)$ are shown in Fig.1 (b). One can see that, except for the larger values of H , the scaling exponents $\alpha(H)$ are in good agreement with the given Hurst numbers. We note that our new method overestimated H for small values of H , and then underestimated it for high

values. We then check the relative error $(\alpha(H) - H)/H$ between given and estimated Hurst number. The corresponding result is shown in Fig.1 (c). Generally speaking, both the kernel smoothing method and the box-counting method provide a comparable estimation of H , especially for a Hurst number around $H = 0.3$. Thus in the following content, we will only apply the box-counting method to real data sets since the scaling exponent is expected around $H = 1/3$.

To test the finite length effect, we perform a calculation with various data length L and 1000 realizations each for the Hurst number $H = 1/3$, this corresponds to the value for fully developed turbulence.³ The range of L is $10^4 < L < 3 \times 10^6$. The corresponding scaling exponents $\alpha(L)$ are estimated on the range $10 < \tau < 1000$ data points. Figure 2 shows $\alpha(L)$ with errorbar $\delta\alpha(L)$, which is the standard deviation of the estimated $\alpha(L)$. The inset shows the relative error $Er(L) = (H - \alpha(L))/H$ (\circ) and the errorbar $\delta\alpha(L)/H$ (\square). Power law behaviors

$$Er(L) \sim (L)^{-\xi}, \quad \delta\alpha(L) \sim L^{-\gamma} \quad (7)$$

are observed with scaling exponents $\xi \simeq 0.91$ and $\gamma \simeq 0.49$. One can find that the estimated α is quickly close to the given Hurst number $H = 1/3$. The relative error $Er(L)$ is less than 10% for all L we considered here. Specifically, when $L > 10^5$, we obtain $Er(L) \leq 1\%$ and $\delta\alpha(L)/H \leq 5\%$. This is already a quite good estimation of H . Thus in the following, we choose $L \geq 10^5$ data points.

B. H -Self-similar processes

We can also derive the pdf scaling more generally for H -self-similar processes as following. We define a H -self-similar process as

$$\{x(at)\} \stackrel{d}{=} \{a^H x(t)\} \quad (8)$$

in which $\stackrel{d}{=}$ means equality in distribution and H is the Hurst number.²⁷ $x(t)$ is a H -self-similar process, in which only one parameter H , namely Hurst number, is required for the above scaling transform. Let us note $Y_\tau = \Delta x_\tau = x(t + \tau) - x(t)$, the increment with separation scale τ . We assume that x is H -self-similar with stationary increment, hence Y_τ is also H -self-similar. Thus one has

$$\left\{ \frac{Y_\tau}{\tau^H} \right\} \stackrel{d}{=} \left\{ \frac{Y_T}{T^H} \right\} \stackrel{d}{=} \{Y_1\} \quad (9)$$

112 In fact equality in distribution means equality for distribution function. Let us write distri-
113 bution function

$$F(x) = P_r(X \leq x) = \int_{-\infty}^x p(X) dX \quad (10)$$

114 in which $p(x)$ is the pdf of x . We note the pdf

$$p(x) = F'(x) \quad (11)$$

115 We thus take here

$$F_\tau(x) = P_r(Y_\tau \leq x) \quad (12)$$

116 We have

$$P_r\left(\frac{Y_\tau}{\tau^H} \leq x\right) = P_r(Y_\tau \leq x\tau^H) \quad (13)$$

117 Hence Eq. (9) writes for distribution functions

$$F_\tau(x\tau^H) = F_T(xT^H) \quad (14)$$

118 Taking the derivative of Eq. (14), we have for the pdfs

$$\tau^H p_\tau(x\tau^H) = T^H p_T(xT^H) \quad (15)$$

119 Then writing

$$p_{\max}(\tau) = \max_x \{p_\tau(x)\} \quad (16)$$

120 and taking the maximum of Eq. (15), we have

$$\tau^H p_{\max}(\tau) = T^H p_{\max}(T) \quad (17)$$

121 Finally, this leads to

$$p_{\max}(\tau) = p_{\max}(T) (\tau/T)^{-H} \quad (18)$$

122 This is the pdf scaling for the H -self-similar process. Since Eq. (8) is not true for multi-
123 scaling processes, Eq. (18) may be only an approximation for multifractal processes.

124 We have shown above analytically the pdf scaling relation for fBm processes and more
125 generally for H -self-similar processes. For the former one, the pdf scaling Eq. (1) is validated
126 by numerical simulations. We postulate here that it is also valid for other types scaling time
127 series, e.g. turbulent velocity and temperature from other turbulent systems, etc., and we
128 will check this experimentally in the next section.

129 The pdf scaling we proposed above is related to the first-order structure function $\alpha =$
 130 H for H -self-similar processes, see Eqs. (5) and (18). Hence for the multifractal case, we
 131 may postulate that $\alpha = \zeta(1)$, the first order structure function with a slight intermittent
 132 correction, see next section for turbulent velocity as an example.

133 III. EXPERIMENTAL RESULTS

134 In this section, we will apply the above pdf scaling analysis to turbulent velocity obtained
 135 from homogeneous and nearly isotropic channel flow, and temperature time series obtained
 136 near sidewall area of a Rayleigh-Bénard convection system. An interpretation under the
 137 K41 theory is also discussed.

138 A. Turbulent velocity

139 We consider here a turbulent velocity database obtained from an experimental homoge-
 140 nous and nearly isotropic turbulent channel flow by using an active-grid technique to achieve
 141 a high Reynolds number.²⁸ We use the data obtained at downstream $x/M = 48$, where M
 142 is the mesh size. At this measurement location, the mean velocity is $\langle u \rangle = 10.8$ m/s, the
 143 turbulence intensity is 10%, and the Taylor microscale based Reynolds number is $Re_\lambda \simeq 630$.
 144 The sampling frequency is 40,000 Hz. To avoid the measurement noise, we only consider
 145 here the transverse velocity. Figure 3 shows the Fourier power spectrum for the transverse
 146 velocity component. The inset shows the compensated spectrum $E(f)f^\beta$, in which $\beta \simeq 1.58$
 147 is the scaling exponent estimated on the range $20 < f < 1000$ Hz, corresponding to the
 148 time separation $0.001 < \tau < 0.05$ s. The value of β for transverse velocity component at all
 149 measurement locations ($x/M = 20, 30, 40, 48$) is around $1.58 \sim 1.60$, and is slightly smaller
 150 than the Kolmogorov value $5/3$, which could be an effect of the active-grid technique.²⁹ It
 151 demonstrates a nearly two decades inertial range. Thus this database has a long enough
 152 inertial range to validate Eq. (1). More details about this database can be found in Ref. 28.

153 $p_{\max}(\tau)$ is calculated as explained below. We first divided the time series into several
 154 segments with 10^5 data points each. Then empirical pdf is estimated for various separation
 155 scales by using Eq. (6). $p_{\max}(\tau)$ is then estimated for each segment. We have $120 \times 12 = 1440$
 156 (number of measurements \times segments of each measurement) realizations. Figure 4 shows

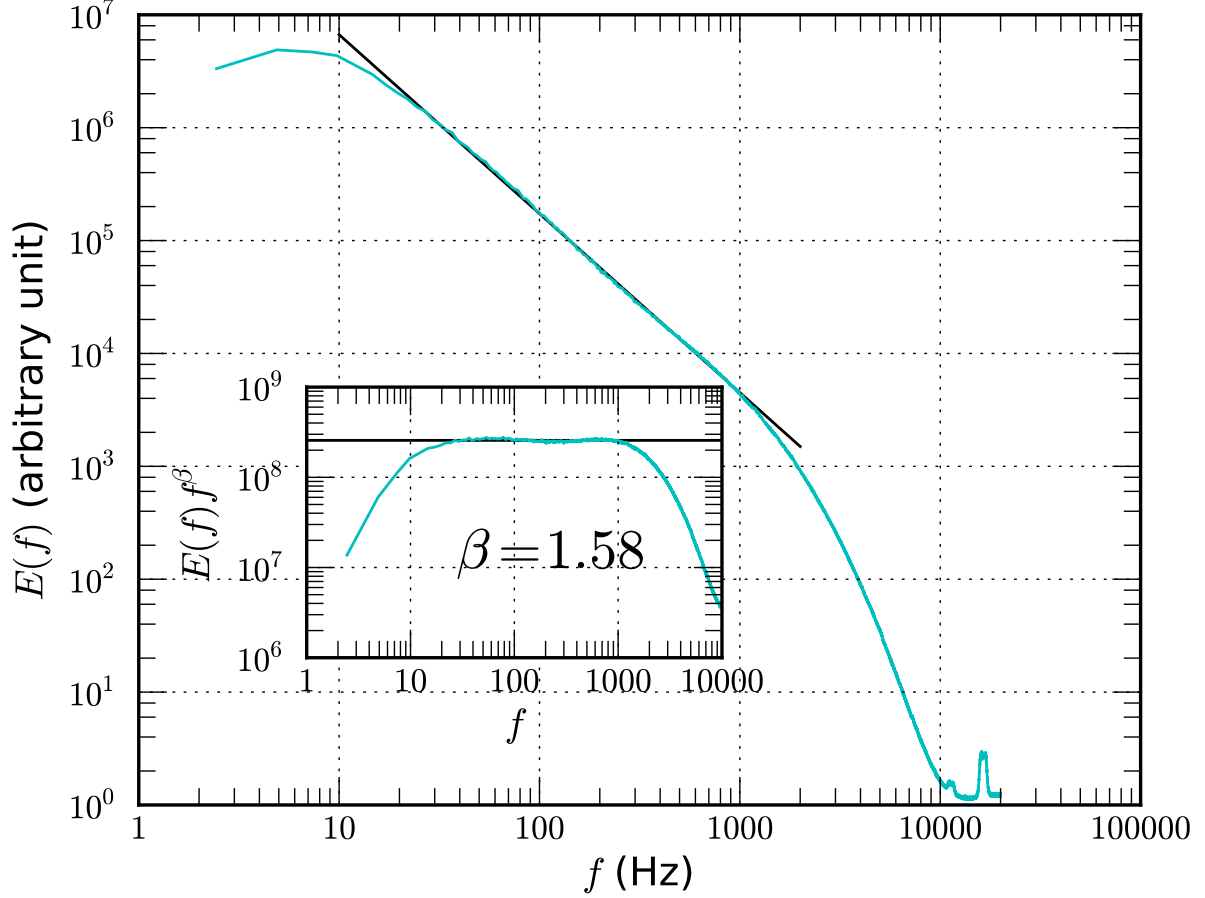


FIG. 3. Fourier power spectrum of transverse velocity component at downstream $x/M = 48$, where M is the mesh size. The inset shows the corresponding compensated spectra $E(f)f^\beta$, where $\beta \simeq 1.58$ is estimated on the range $20 < f < 1000$ Hz, corresponding to the time separation τ on the range $0.001 < \tau < 0.05$ s.

the estimated pdf for several separation scales τ for one realization. The location of maxima pdf $p_{\max}(\tau)$ is marked by \times . Graphically, $p_{\max}(\tau)$ decreases with τ and the corresponding location is around, not exactly, $Y_\tau = 0$. Figure 5 shows (a) the pdf of p_{\max} for several separation scales τ , (b) $X = \log_{10}(p_{\max})$, (c) the skewness factor of p_{\max} and $\log_{10}(p_{\max})$, and (d) the flatness factor. The separation scales in Fig. 5 (a) and (b) are $\tau = 0.0005$ (■), 0.01 (●) and $\tau = 0.1$ s (▲), corresponding to $f = 2000$ Hz in dissipation range, 100 Hz in inertial range and 10 Hz in large scale forcing range, respectively. Both normal and lognormal fits seem to capture the fluctuations of $p_{\max}(\tau)$. It seems that the lognormal fit is better than the normal one, but more data are certainly needed to remove measurement uncertainty and to determine without ambiguity which pdf fit is closest to the data.

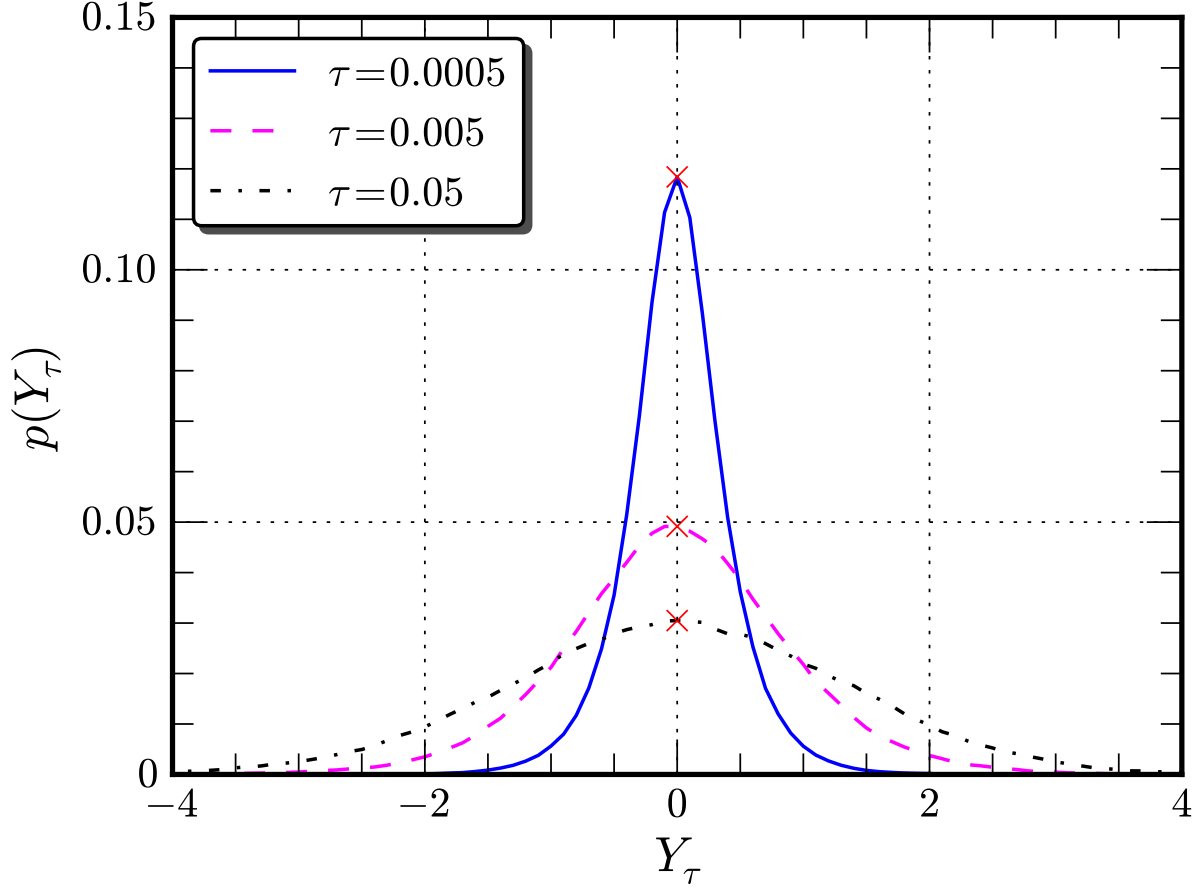


FIG. 4. Empirical pdf estimated for transverse velocity with time separation $\tau = 0.0005$, 0.005 , and 0.05 s, corresponding to $f = 2000$, 200 and 20 Hz. The location for $p_{\max}(\tau)$ is marked by \times .

Figure 6 shows the ensemble averaged $p_{\max}(\tau)$ for the transverse velocity (\circ). The inset shows the local slope, in which the horizontal solid line illustrates the Kolmogorov value $1/3$ and the dashed line illustrates the value 0.37 , and the vertical solid line demonstrates the plateau range, e.g. the inertial range $0.001 < \tau < 0.01$ s. Here the local slope is defined as

$$\alpha(\tau) = -\frac{d \log_{10}(p_{\max}(\tau))}{d \log_{10}(\tau)} \quad (19)$$

A power law behavior is observed over the range $0.001 < \tau < 0.01$ s, corresponding to the frequency range $100 < f < 1000$ Hz. This inertial range can be also confirmed by the plateau of the local slope. The scaling exponent is found to be $\alpha \simeq 0.37$, which is obtained by a least square fitting algorithm. It is interesting to note that this value is consistent with the scaling exponent of the first-order SFs reported in other studies,^{6,30,31} indicating almost the same intermittent correction on the probability space and the statistical moments space. For comparison, the first-order SF $S_1(\tau) = \langle |Y_\tau| \rangle$ is also shown as \triangle . Note that the absolute

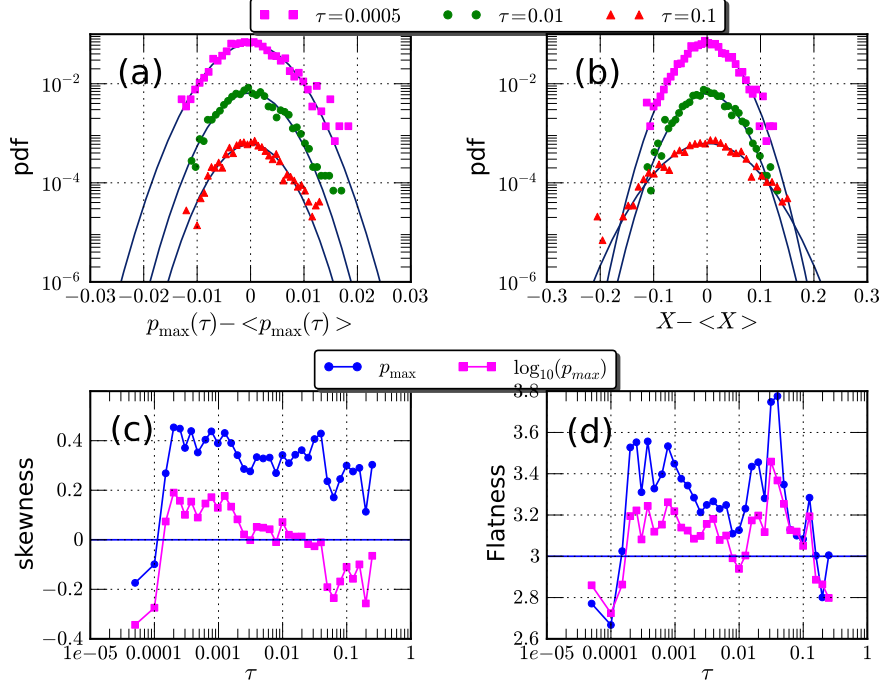


FIG. 5. (a) pdf of $p_{\max}(\tau)$, (b) pdf of $X = \log_{10}(p_{\max}(\tau))$, and (c) the skewness factor of p_{\max} (●) and $\log_{10}(p_{\max})$, and (d) the flatness factor. Separation scales in (a) and (b) are $\tau = 0.0005$ s (■), 0.01 s (●) and $\tau = 0.1$ s (▲), corresponding to $f = 2000$ Hz in dissipation range, 100 Hz in inertial range, and 10 Hz in large scale forcing range, respectively. For display convenience in (a) and (b), the mean value of each scale is removed and the curves have been vertically shifted. The normal distribution is illustrated by a solid line.

value of increments does not change the result of this paper. For display convenience, it has been converted by taking $1/S_1(\tau)$. It predicts the same inertial range as $p_{\max}(\tau)$. The corresponding scaling exponent is found to be $\zeta(1) \simeq 0.34$, very close to the Kolmogorov value $1/3$. One can find that the $p_{\max}(\tau)$ shows a behavior which seems more linear than $S_1(\tau)$ on the inertial range, see also Fig. 7 for temperature data. This is because the first-order SF $S_1(\tau)$ is more sensitive to large-scale structures, which might pollute the whole inertial range, see the discussion below and an example of passive scalars with large-scale ramp-cliff structures in Ref. 32.

We note that the inertial range predicted by Fourier power spectrum $E(f)$ is different from the one predicted by first-order SF $S_1(\tau)$ and $p_{\max}(\tau)$. This phenomenon has been reported by several authors for the second-order SF $S_2(\tau)$ and the Fourier power spectrum

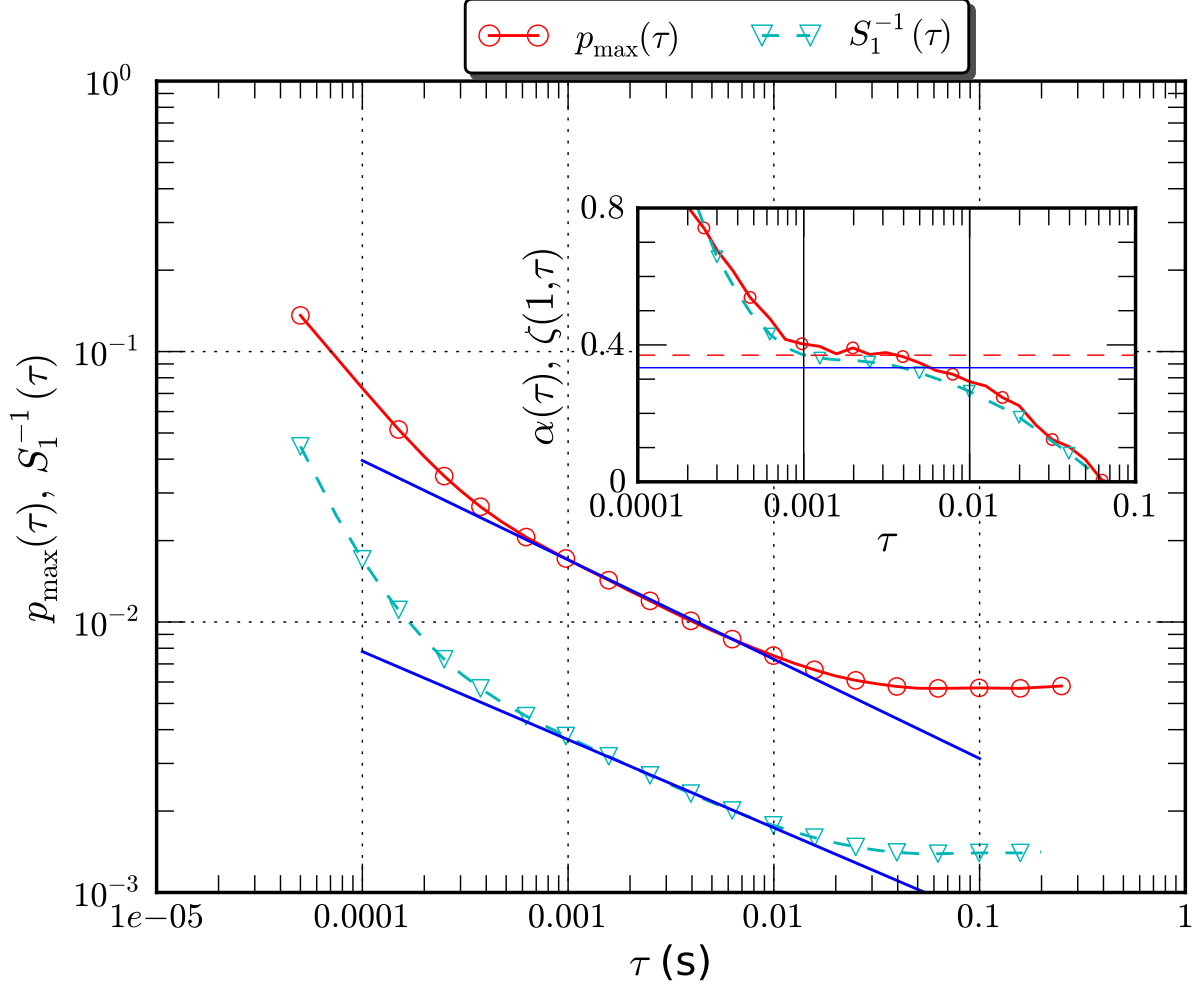


FIG. 6. $p_{\max}(\tau)$ and the first-order structure function $S_1(\tau)$ of transverse velocity component. The scaling exponents are $\alpha \simeq 0.37$ and $\zeta(1) \simeq 0.34$ estimated on the power law range $0.001 < \tau < 0.01$ s, corresponding to $100 < f < 1000$ Hz. The inset shows the local slope $\alpha(\tau)$ and $\zeta(1, \tau)$, in which the horizontal solid line indicates the Kolmogorov value $1/3$, and the dashed line indicates the value 0.37 , and the vertical solid line illustrates the inertial range. For display convenience, we have shown the inverse value $1/S_1(\tau)$ of the first-order structure function and the curves have been vertically shifted.

¹⁸⁹ $E(f)$.^{3,24,32–34} If one considers the Wiener-Khinchin theorem,^{3,32,35} $S_2(\tau)$ and $E(f)$ can be
¹⁹⁰ related to each other as

$$S_2(\tau) = \int_0^{+\infty} E(f) (1 - \cos(2\pi\tau f)) \, df \quad (20)$$

¹⁹¹ Therefore, for a scaling time series, they are expected to have the same inertial range, and

the corresponding scaling exponents are related as $\beta = 1 + \zeta(2)$. The difference may come from the following reasons: (i) the finite power law range,^{32,34} (ii) the spectrum of the original velocity is not a pure power law,^{3,33} (iii) violation of the statistical stationary assumption, and (iv) also the influence of large-scale structures.^{32,36} More detail of the discussion can be

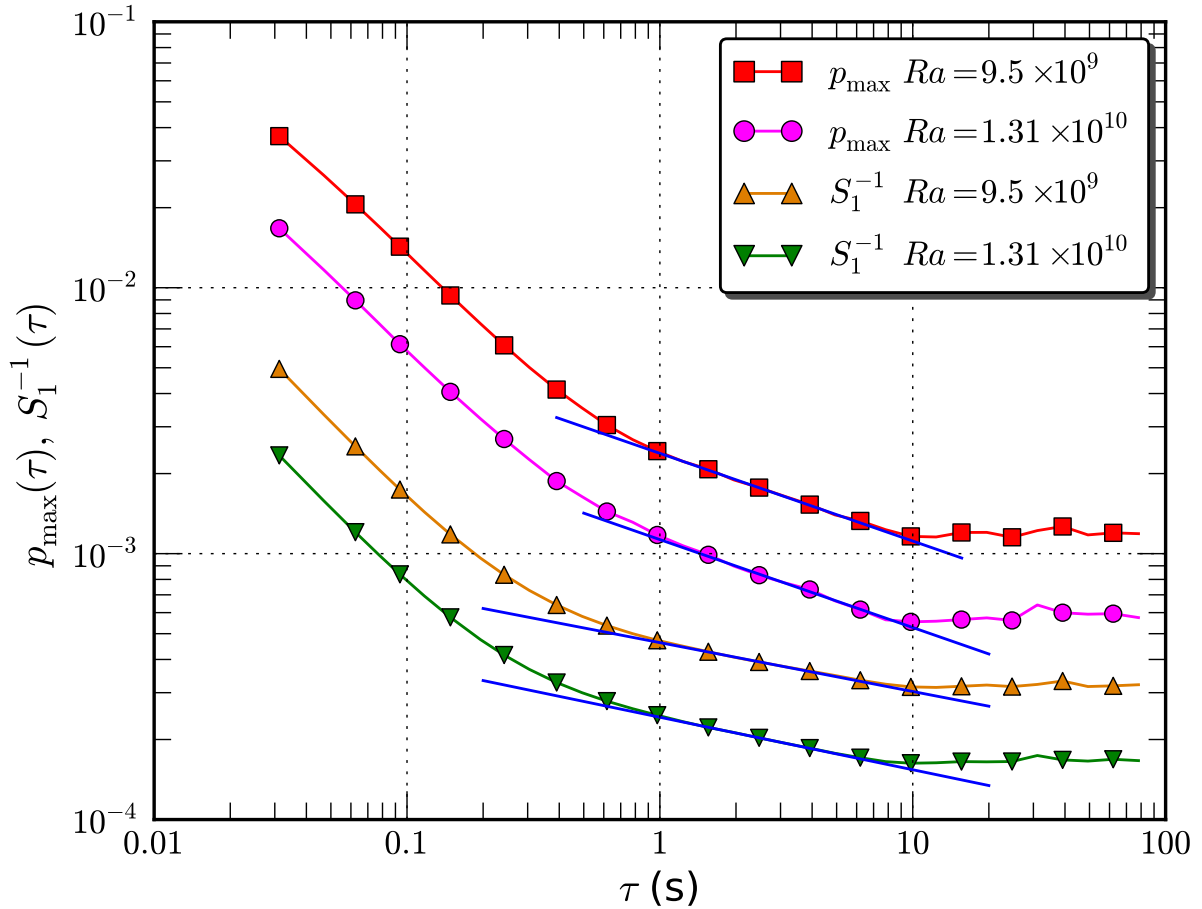


FIG. 7. $p_{\max}(\tau)$ and the first-order structure functions $S_1^\theta(\tau)$ of temperature. Power law behavior is found over the range $1 < \tau < 10$ s for all curves. The corresponding scaling exponents are $\alpha_\theta \simeq 0.33$ and $\zeta_\theta(1) \simeq 0.19$, respectively. For display convenience, we have shown the inverse value $1/S_1^\theta(\tau)$ of the first-order structure function and the curves have been vertically shifted.

We finally consider a temperature data sets obtained near the sidewall of turbulent RBC

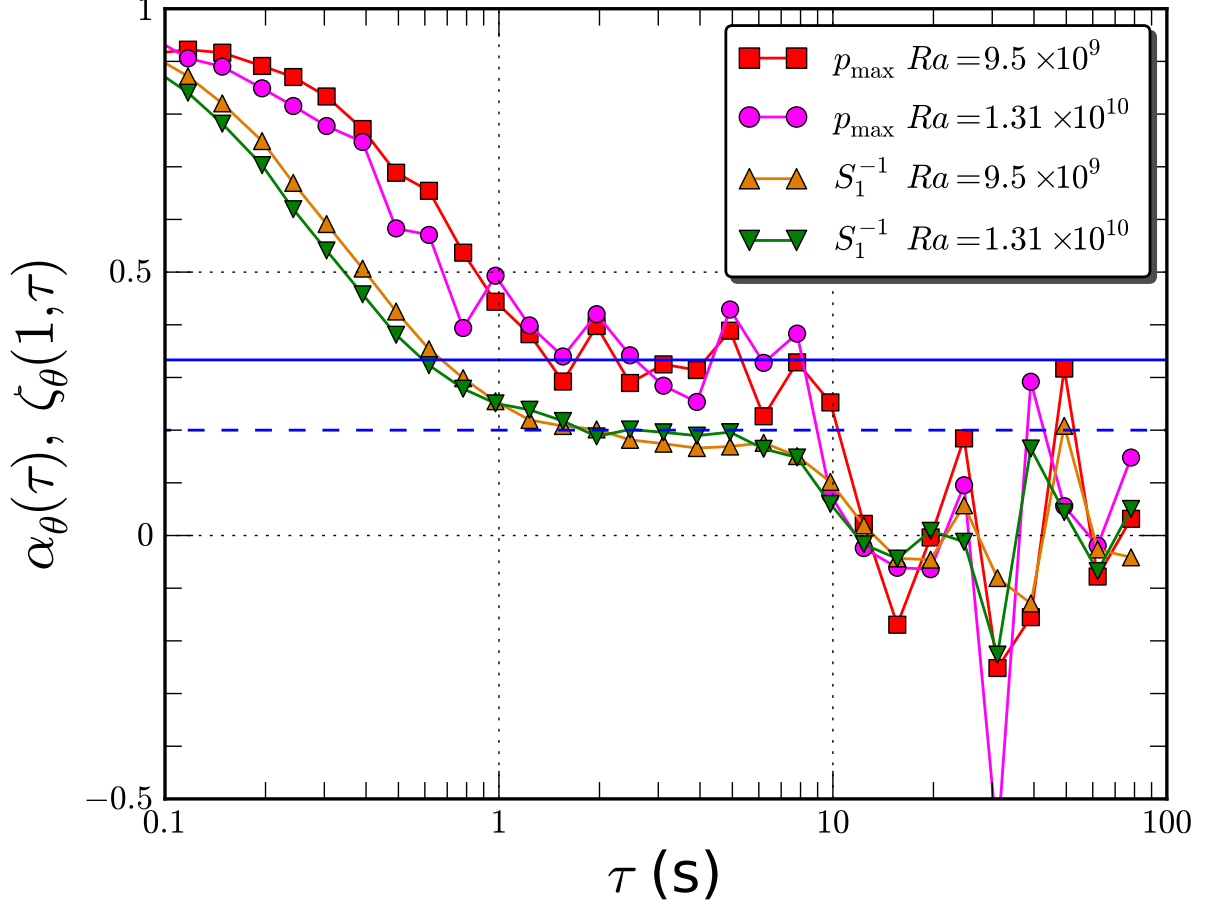


FIG. 8. Local slope for the $p_{\max}(\tau)$ and $S_1^{-1}(\tau)$. The solid horizontal line is the KOC scaling $1/3$, and the dashed line is the BO59 scaling $1/5$.

199 system. The experiments were performed by Prof. Xia's group in the Chinese University
 200 of Hong Kong. The details of the experiments have been described elsewhere.^{37–39} Briefly,
 201 the temperature measurements were carried out in a cylindrical cell with upper and lower
 202 copper plates and Plexiglas sidewall. The inner diameter of the cell is $D = 19.0$ cm and
 203 the height is $L = 19.6$ cm. So its aspect ratio is $\Gamma = D/L \simeq 1$. Water was used as
 204 the working fluid and measurement were made at Rayleigh number $Ra = 9.5 \times 10^9$ and
 205 1.31×10^{10} . During the experiments, the entire cell was placed inside a thermostat box
 206 whose temperature matches the mean temperature of the bulk fluid that was kept at $\sim 40^\circ\text{C}$,
 207 corresponding to a Prandtl number $Pr = 4.4$. The local temperature was measured at 8
 208 mm from the sidewall at midheight by using a small thermistor of 0.2 mm diameter and 15
 209 ms time constant. Typically, each measurement of temperature lasted 20 h or longer with a

210 sampling frequency 64 Hz, ensuring that the statistical averaging is adequate.

211 Near the sidewall of a turbulent convection cell, the turbulent flow is driven by buoyancy
212 in the vertical direction. As proposed by Bolgiano and Obukhov, there is a typical length
213 scale in buoyancy-driven turbulence, now commonly referred to as the Bolgiano scale L_B ,
214 above which buoyancy effects are important and the Bolgiano-Obukhov (BO59) scaling
215 $E_\theta(k) \sim k^{-7/5}$ for temperature power spectrum or $S_q^\theta(r) \sim r^{q/5}$ for SFs are expected.^{5,40}
216 Whether the BO59 scaling exists in turbulent RBC system has been studied extensively in
217 the past two decades, whereas it remains a major challenge to settle this problem (see, for a
218 recent review, Ref. 5). Nevertheless, it has been shown recently that above a certain scale
219 buoyancy effects indeed become predominant, at least in the time domain.^{41,42} The observed
220 Bolgiano time scale here is of order 1 second.^{41–43}

221 Figure 7 and 8 show respectively the estimated $p_{\max}(\tau)$ and the first-order SFs $S_1^\theta(\tau)$,
222 and the local slope, in which dashed line indicates the BO59 scaling 1/5 and the solid line
223 indicates the KOC scaling 1/3. One can see the power-law behaviors or the plateaus above
224 the Bolgiano time scale, i.e. on the range $1 < \tau < 10$ s. For pdfs, the fitted scaling exponent
225 is $\alpha_\theta \simeq 0.33$, which is almost the same as the Kolmogorov-Obukhov-Corrsin (KOC) value of
226 $1/3$ for passive scalar,^{3,44} whereas for SFs, the fitted scaling exponent $\zeta_\theta(1) \simeq 0.19$, which is
227 very close to the BO59 value of $1/5$. At first glance, these results seem to be contradicting and
228 confusing. To understand this, we note that in turbulent RBC buoyant forces are exerted on
229 the fluid mainly via thermal plumes. As revealed by several visualizations, thermal plumes
230 consist of a front with sharp temperature gradient and hence these thermal structures would
231 induce intense temperature increments, which correspond to the pdf tails.^{45–47} Therefore, it
232 is not surprising that $p_{\max}(\tau)$ investigated here could not capture efficiently the information
233 of thermal plumes and thus may preclude buoyancy effects. See next section for more
234 discussion.

235 Note that the Taylor’s frozen-flow hypothesis,

$$r_T = -\langle u \rangle \tau, \quad (21)$$

236 is always used to relate the time domain results, such as those shown in Fig. 7, to the
237 theoretical predictions made for the space domain. However, the conditions for the Taylor’s
238 hypothesis are often not met in turbulent RBC system and hence its applicability to the
239 system is at best doubtful.^{5,48,49} Recently, based on a second order approximation, He and

coworkers^{50,51} advanced an elliptic model for turbulent shear flows. Later, the model was validated in turbulent RBC system indirectly using the temperature data by Tong and coworkers^{52,53} and directly using the velocity data by Zhou *et al.*⁵⁴. The most important implication of the elliptic model is that the model can be used to translate time series to space series via

$$r_E = -(U^2 + V^2)^{1/2} \tau \quad (22)$$

where U is a characteristic convection velocity proportional to the mean velocity and V is a characteristic velocity associated with the r.m.s. velocity and the shear-induced velocity. As pointed by Zhou *et al.*⁵⁴, r is proportional to τ for both the Taylor's relation Eq. (21) and the elliptic relation Eq. (22), but the proportionality constants of the two relations are different. This implies that the Taylor's hypothesis and elliptic model would yield the same scaling exponents. Therefore, if one is only interested in the scaling exponents, one does not really need the validity of Taylor's hypothesis to reconstruct the space series from the

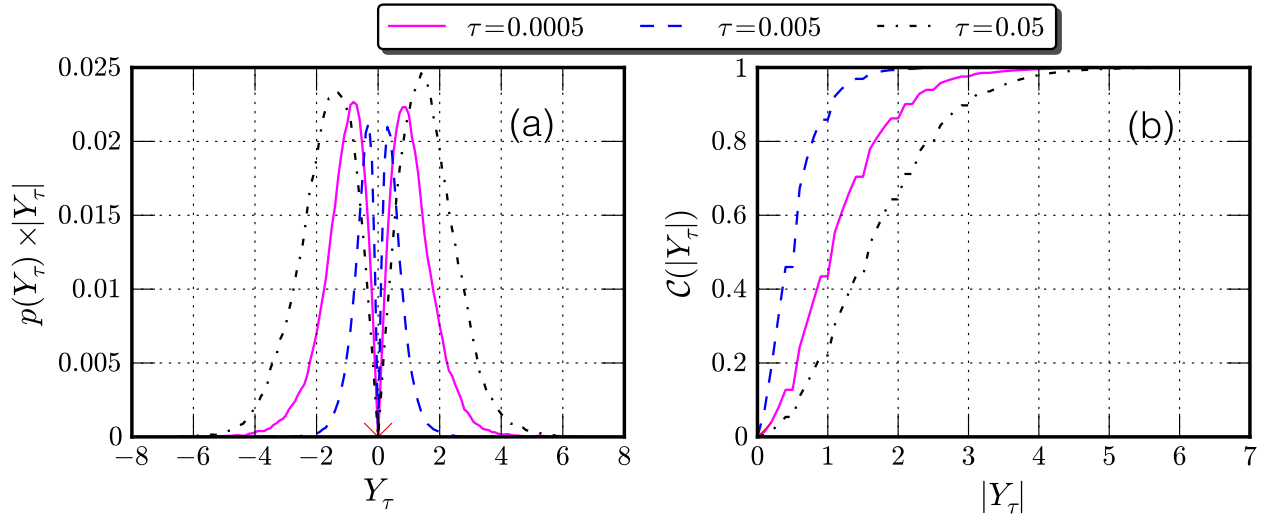


FIG. 9. (a) the integral kernel of first-order structure function, and (b) the normalized cumulative function $\mathcal{C}(|Y_\tau|)$. The location of $p_{\max}(\tau)$ is at $Y_\tau \simeq 0$ and marked by \times .

We have mentioned above that for the turbulent velocity the inertial range predicted by

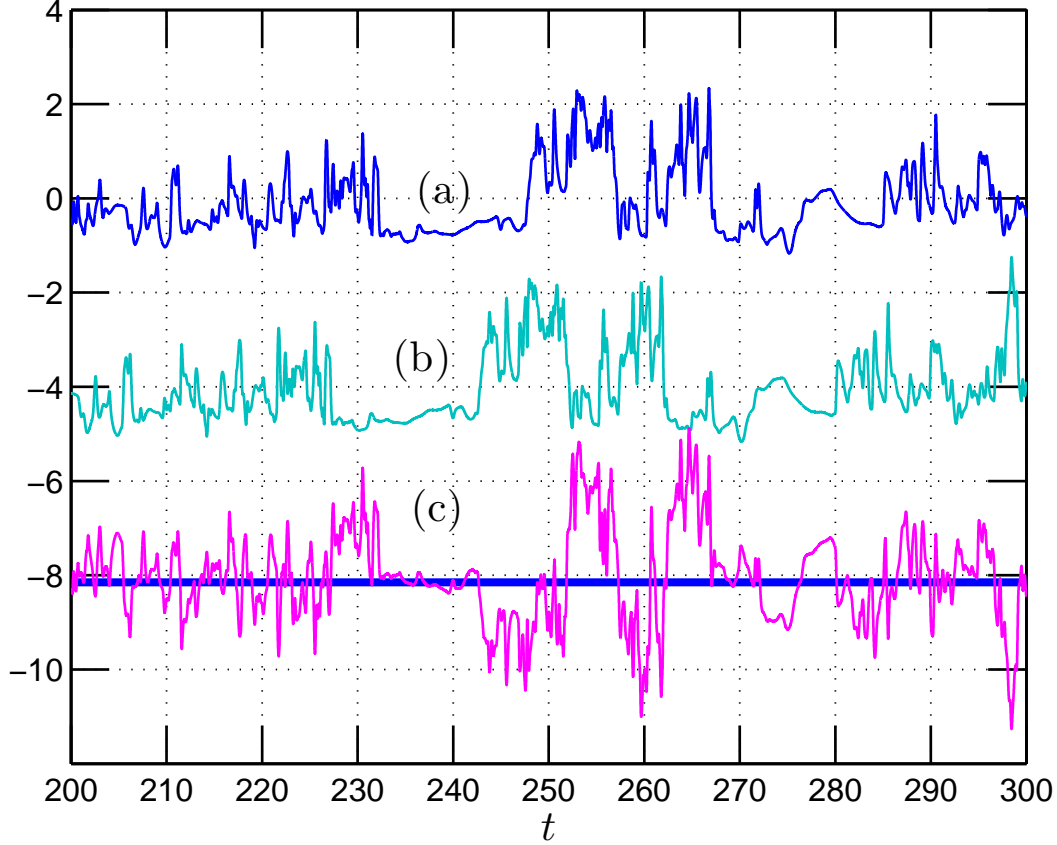


FIG. 10. Demonstration of the influence of large-scale structures (plume). They are (a) a portion of temperature data $\theta(t)$, (b) $\theta(t + \tau)$, and (c) increment $Y_\tau^\theta(t)$ with $\tau = 5$ s, respectively. The p_{\max} is located at $Y_\tau^\theta \simeq -0.15$, which is indicated by a small horizontal patch. For clarity, the curves have been vertical shifted.

Fourier power spectrum $E(f)$ is larger than those predicted by the $p_{\max}(\tau)$ and by the first-order SF. Indeed, it has been reported by several authors that the inertial range predicted by the second-order SF $S_2(\tau)$ is shorter than Fourier power spectrum.^{3,4,33,34} By taking an assumption of statistical stationary and Wiener-Khinchin theorem, $S_2(\tau)$ and $E(f)$ can be related with each other,^{3,35} see Eq. (20). Thus both methods are expected to predict an identical inertial range.^{3,4} However, the statement of the Wiener-Khinchin theorem only exactly holds for a stationary process, which may be not satisfied by the turbulent velocity.

As pointed by Huang *et al.*³², the second-order SF is also strongly influenced by the large-scale structures. We show this point experimentally here. A more rigorous discussion can be found in Ref. 32. Figure 9 shows (a) the integral kernel $p(Y_\tau) \times |Y_\tau|$ of the first-order

265 SF for three same separation scales as in Fig. 4 (a), and (b) the corresponding normalized
 266 cumulative function $\mathcal{C}(|Y_\tau|)$, respectively. The location of $p_{\max}(\tau)$ is marked as \times . The
 267 normalized cumulative function $\mathcal{C}(|Y_\tau|)$ is defined as

$$\mathcal{C}(|Y_\tau|) = \frac{\int_{-Y_\tau}^{Y_\tau} p(Y'_\tau) |Y'_\tau| dY'_\tau}{\int_{-\infty}^{\infty} p(Y'_\tau) |Y'_\tau| dY'_\tau} \quad (23)$$

268 It characterizes the relative contribution to the first-order SF. The location of p_{\max} is found
 269 graphically to be $Y_\tau \simeq 0$, indicating that at this location there is almost no contribution to
 270 SFs. If we consider the large index value of Y_τ coming from large-scale structures, most of
 271 the contribution to SFs comes from them. The contribution is found also to be increased
 272 with the increase of τ , see Fig. 9 (b). Thus p_{\max} is less influenced by large-scale structures,
 273 revealing a more accurate scaling exponent for $\zeta(1)$.

274 In the sidewall region of RBC system, the flow is dominated by plumes.^{5,40} Figure 10
 275 shows (a) a portion of temperature data $\theta(t)$, (b) $\theta(t + \tau)$, and (c) increment Y_τ^θ with
 276 $\tau = 5$ s, respectively. Due to the presence of plumes, the shape of pdf $p(Y_\tau^\theta)$ is asymmetric
 277 (not shown here).⁴² The location of p_{\max} is at $Y_\tau^\theta \simeq -0.15$, which is indicated as a small
 278 horizontal patch. For SFs, they include contribution from all scale structures. On the
 279 contrary, p_{\max} acts a kind of conditional statistic, in which the contribution from large-scale
 280 structures, e.g. thermal plumes, is excluded, see Fig. 10 (c). The large-scale structures
 281 here are believed to be thermal plumes. Thus the scaling of p_{\max} may represent the scaling
 282 property of the background fluctuation, which is believed to satisfy KOC scaling.^{5,40} Indeed,
 283 the KOC scaling for the first-order statistical moment has been found by using a generalized
 284 autocorrelation function of the increment, which confirms the idea that in the sidewall region
 285 the temperature fluctuation can be considered as a KOC background fluctuation superposed
 286 to BO59 fluctuations (thermal plumes).

287 This result is compatible with the Grossmann-Lohse (GL) theory,^{55–57} in which the global
 288 thermal dissipation ϵ_θ is decomposed into the thermal dissipation due to the bulk $\epsilon_{\theta,bulk}$
 289 together with the boundary layer $\epsilon_{\theta,BL}$

$$\epsilon_\theta = \epsilon_{\theta,bulk} + \epsilon_{\theta,BL} \quad (24)$$

290 Later, the GL theory has been modified so that the thermal dissipation ϵ_θ can be decomposed
 291 into the thermal dissipation due to the thermal plumes $\epsilon_{\theta,pl}$ together with the turbulent

background $\epsilon_{\theta,bg}$ ⁵⁸

$$\epsilon_{\theta} = \epsilon_{\theta,pl} + \epsilon_{\theta,bg} \quad (25)$$

in which the contribution from the thermal plumes might be related to the boundary layer. Therefore, in the sidewall region, the thermal dissipation is dominated by the thermal plumes (or boundary layer), see more details in Ref. 58. More recently, this picture has been proofed to be correct at least in the central region of the RBC system by Ni, Huang, and Xia⁵⁹. Our result here indicates that in the sidewall region, the turbulent background should have contribution to the global thermal dissipation as well as the thermal plumes. Or in other words, the KOC and BO59 scalings might coexist at least for the temperature fluctuations. We will show this result elsewhere.

The method we proposed here may be refined by considering some pdf models as basis, e.g. Eq.(3.8) in Ref. 8. However, it seems that the Eq.(3.8) requires the resolution of the spatial dissipation scale η to determine a parameter σ_0 , the most probable variance of conditional velocity u at a given dissipation rate ϵ , see more details in Ref. 8. Unfortunately, the data set we have has no resolution on dissipation scale.²⁸ More data sets and pdf models will be considered in future studies to refine our method.

One advantage of the present method to consider scaling properties of time series is its ability to exclude the influence of large-scale structure as much as possible. Indeed, we have observed a Kolmogorov-like pdf scaling for other data set, in which other moment-based methods do not detect the power-law behavior. It is believed that the scaling is destroyed by large-scale structures (result not shown here).

In summary, we investigated the pdf scaling of velocity increments $Y_{\tau}(t)$. We postulated a scaling relation of the maxima value of the pdfs, e.g. $p_{\max}(\tau) \sim \tau^{-\alpha}$. We obtained this scaling relation analytically for fBm processes and more generally for H -self-similar processes with $\alpha = \zeta(1)$. For the former one, it has been validated by fBm simulations. The pdf scaling exponent α is comparable with the scaling exponent $\zeta(1)$ of the first-order SFs. To our knowledge, at least for H -self-similar processes, this is the first method to look at scaling properties on the probability space rather than on the statistical moments space as done classically. We postulated that the pdf scaling holds for multifractal processes as well. For multifractal processes, due to the failure of Eq. (8), the scaling relation may be only an approximation.

When applying this approach to turbulent velocity, it is found that, statistically speaking,

$p_{\max}(\tau)$ satisfies both normal and lognormal distributions. A scaling exponent $\alpha \simeq 0.37$ is found experimentally which is consistent with the scaling exponent $\zeta(1)$ of the first-order SFs reported in other studies, indicating the same intermittent correction on both the probability space and the statistical moments space. For temperature near the sidewall of RBC system, the scaling exponent is found to be $\alpha_\theta \simeq 0.33$. This value is in favor of KOC scaling for passive scalar, not BO59 scaling. It indicates that the KOC scaling may be extracted by a proper designed method. We show experimentally that the contribution of plumes to p_{\max} is almost excluded, whereas the SF contains contributions from both small-scale and larger-scale structures. Indeed the contribution from the former ones is much smaller than from the later ones. Thus the pdf scaling exponent α_θ represents the scaling property of the background flow. In other words, the temperature fluctuation in the side wall region of a RBC can be considered as a KOC background fluctuation superposed to BO59 fluctuations (thermal plumes). The first-order KOC scaling exponent has been confirmed by using other approach. The potential application of these new findings may serve as a constrain of some turbulent models, for example, the pdf model (Eq. (3.8)) in Ref. 8.

ACKNOWLEDGMENTS

This work is sponsored in part by the Key Project of Shanghai Municipal Education Commission (No. 11ZZ87) and the Shanghai Program for Innovative Research Team in Universities and in part by the National Natural Science Foundation of China under Grant Nos. 10772110 and 11072139. X.S. thanks the financial support from the National Natural Science Foundation of China under No. 10972229 and U1033002. Y. H. thanks Prof. S.Q. Zhou in SCSIO for useful discussion. We thank Prof. K.-Q. Xia from Chinese University of Hongkong for providing us the temperature data. We also thank Prof. Meneveau for sharing his experimental velocity database, which is available for download at C. Meneveau's web page: <http://www.me.jhu.edu/meneveau/datasets.html>. We also thank the anonymous referees for their useful suggestions.

REFERENCES

- ¹A. N. Kolmogorov, “Local structure of turbulence in an incompressible fluid at very high Reynolds numbers,” Dokl. Akad. Nauk SSSR **30**, 301 (1941).
- ²F. Anselmet, Y. Gagne, E. J. Hopfinger, and R. A. Antonia, “High-order velocity structure functions in turbulent shear flows,” J. Fluid Mech. **140**, 63–89 (1984).
- ³U. Frisch, *Turbulence: the legacy of AN Kolmogorov* (Cambridge University Press, 1995).
- ⁴K. Sreenivasan and R. Antonia, “The phenomenology of small-scale turbulence,” Annu. Rev. Fluid Mech. **29**, 435–472 (1997).
- ⁵D. Lohse and K.-Q. Xia, “Small-scale properties of turbulent rayleigh-bénard convection,” Ann. Rev. Fluid Mech. **42**, 335–364 (2010).
- ⁶A. Arneodo, C. Baudet, F. Belin, R. Benzi, B. Castaing, B. Chabaud, R. Chavarria, S. Ciliberto, R. Camussi, and F. Chilla, “Structure functions in turbulence, in various flow configurations, at Reynolds number between 30 and 5000, using extended self-similarity,” Europhys. Lett. **34**, 411–416 (1996).
- ⁷A. S. Monin and A. M. Yaglom, *Statistical fluid mechanics vd II* (MIT Press Cambridge, Mass, 1971).
- ⁸B. Castaing, Y. Gagne, and E. Hopfinger, “Velocity probability density functions of high Reynolds number turbulence,” Physica D **46**, 177–200 (1990).
- ⁹E. Ching, “Probabilities for temperature differences in rayleigh-bénard convection,” Phys. Rev. A **44**, 3622 (1991).
- ¹⁰P. Kailasnath, K. Sreenivasan, and G. Stolovitzky, “Probability density of velocity increments in turbulent flows,” Phys. Rev. Lett. **68**, 2766–2769 (1992).
- ¹¹E. Ching, “Probability densities of turbulent temperature fluctuations,” Phys. Rev. Lett. **70**, 283–286 (1993).
- ¹²P. Tabeling, G. Zocchi, F. Belin, J. Maurer, and H. Willaime, “Probability density functions, skewness, and flatness in large reynolds number turbulence,” Phys. Rev. E **53**, 1613 (1996).
- ¹³A. Noullez, G. Wallace, W. Lempert, R. Miles, and U. Frisch, “Transverse velocity increments in turbulent flow using the RELIEF techniques,” J. Fluid Mech. **339**, 287–307 (1997).
- ¹⁴A. Kolmogorov, “The Wiener spiral and some other interesting curves in Hilbert space,”

380 *Dokl. Akad. Nauk SSSR*, Dokl. Akad. Nauk SSSR **26**, 115–118 (1940).

381 ¹⁵A. Yaglom, “Some classes of random fields in n -dimensional space, related to stationary
382 random processes,” *Theor. Probab. App+* **2**, 273 (1957).

383 ¹⁶B. Mandelbrot and J. Van Ness, “Fractional Brownian Motions, Fractional Noises and
384 Applications,” *SIAM Review* **10**, 422 (1968).

385 ¹⁷P. Flandrin, “Wavelet analysis and synthesis of fractional Brownian motion,” *IEEE Trans.*
386 *Inf. Theory* **38**, 910–917 (1992).

387 ¹⁸G. Samorodnitsky and M. Taqqu, *Stable Non-Gaussian Random Processes: stochastic*
388 *models with infinite variance* (Chapman & Hall, 1994).

389 ¹⁹J. Beran, *Statistics for long-memory processes* (CRC Press, 1994).

390 ²⁰L. Rogers, “Arbitrage with Fractional Brownian Motion,” *Math. Finance* **7**, 95–105 (1997).

391 ²¹P. Doukhan, M. Taqqu, and G. Oppenheim, *Theory and Applications of Long-Range*
392 *Dependence* (Birkhauser, 2003).

393 ²²C. W. Gardiner, *Handbook of Stochastic Methods* (Springer, Berlin, third edition, 2004).

394 ²³F. Biagini, Y. Hu, B. Oksendal, and T. Zhang, *Stochastic calculus for fractional Brownian*
395 *motion and applications* (Springer Verlag, 2008).

396 ²⁴Y. Huang, F. G. Schmitt, Z. Lu, and Y. Liu, “Autocorrelation function of velocity incre-
397 ments in fully developed turbulence,” *Europhys. Lett.* **86**, 40010 (2009).

398 ²⁵P. Abry and F. Sellan, “The Wavelet-Based synthesis for fractional Brownian motion
399 proposed by F. Sellan and Y. Meyer: remarks and fast implementation,” *Appl. Comput.*
400 *Harmon. Anal.* **3**, 377–383 (1996).

401 ²⁶M. Wand and M. Jones, *Kernel smoothing* (Chapman & Hall/CRC, 1995).

402 ²⁷P. Embrechts and M. Maejima, *Self-similar processes* (Princeton University Press, 2002).

403 ²⁸H. Kang, S. Chester, and C. Meneveau, “Decaying turbulence in an active-grid-generated
404 flow and comparisons with large-eddy simulation,” *J. Fluid Mech.* **480**, 129–160 (2003).

405 ²⁹However, for the second-order structure functions, the corresponding scaling exponent is
406 $\zeta(2) \simeq 0.64$ (the figure not shown here). It indicates that the relation $\beta = 1 + \zeta(2)$ does
407 not hold, which has been understood as an effect of large-scale structure and finite scaling
408 range. Another example for passive scalar has been shown in Ref. 32.

409 ³⁰R. Benzi, S. Ciliberto, R. Tripiccion, C. Baudet, F. Massaioli, and S. Succi, “Extended
410 self-similarity in turbulent flows,” *Phys. Rev. E* **48**, 29–32 (1993).

411 ³¹Z. S. She and E. L  v  que, “Universal scaling laws in fully developed turbulence,” *Phys.*

412 Rev. Lett. **72**, 336–339 (1994).

413 ³²Y. Huang, F. G. Schmitt, Z. Lu, P. Fougairolles, Y. Gagne, and Y. Liu, “Second-order
414 structure function in fully developed turbulence,” Phys. Rev. E **82**, 26319 (2010).

415 ³³M. Nelkin, “Universality and scaling in fully developed turbulence,” Adv. Phys. **43**, 143–
416 181 (1994).

417 ³⁴T. Hou, X. Wu, S. Chen, and Y. Zhou, “Effect of finite computational domain on tur-
418 bulence scaling law in both physical and spectral spaces,” Phys. Rev. E **58**, 5841–5844
419 (1998).

420 ³⁵D. Percival and A. Walden, *Spectral Analysis for Physical Applications: Multitaper and*
421 *Conventional Univariate Techniques* (Cambridge University Press, 1993).

422 ³⁶Y. Huang, *Arbitrary-Order Hilbert Spectral Analysis: Definition and Application to*
423 *fully developed turbulence and environmental time series*, Ph.D. thesis, Université des
424 Sciences et Technologies de Lille - Lille 1, France & Shanghai University, China
425 (2009)<http://tel.archives-ouvertes.fr/tel-00439605/fr>.

426 ³⁷X.-D. Shang, X.-L. Qiu, P. Tong, and K.-Q. Xia, “Measured local heat transport in
427 turbulent Rayleigh-Bénard convection,” Phys. Rev. Lett. **90**, 074501 (2003).

428 ³⁸X.-D. Shang, X.-L. Qiu, P. Tong, and K.-Q. Xia, “Measurements of the local convective
429 heat flux in turbulent Rayleigh-Bénard convection,” Phys. Rev. E **70**, 026308 (2004).

430 ³⁹X.-D. Shang, P. Tong, and K.-Q. Xia, “Scaling of the local convective heat flux in turbulent
431 Rayleigh-Bénard convection,” Phys. Rev. Lett. **100**, 244503 (2008).

432 ⁴⁰G. Ahlers, S. Grossmann, and D. Lohse, “Heat transfer and large scale dynamics in
433 turbulent Rayleigh-Bénard convection,” Rev. Mod. Phys. **81**, 503–537 (2009).

434 ⁴¹E. S. C. Ching, K.-W. Chui, X.-D. Shang, X.-L. Qiu, P. Tong, and K.-Q. Xia, “Velocity
435 and temperature cross-scaling in turbulent thermal convection,” J. Turbu. **5**, 027 (2004).

436 ⁴²Q. Zhou and K.-Q. Xia, “Comparative experimental study of local mixing of active and
437 passive scalars in turbulent thermal convection,” Phys. Rev. E **77**, 056312 (2008).

438 ⁴³S.-Q. Zhou and K.-Q. Xia, “Scaling properties of the temperature field in convective tur-
439 bulence,” Phys. Rev. Lett. **87**, 064501 (2001).

440 ⁴⁴Z. Warhaft, “Passive scalars in turbulent flows,” Annu. Rev. Fluid Mech. **32**, 203–240
441 (2000).

442 ⁴⁵J. Zhang, S. Childress, and A. Libchaber, “Non-Boussinesq effect: Thermal convection
443 with broken symmetry,” Phys. Fluids **9**, 1034–1042 (1997).

⁴⁴⁴ ⁴⁶H.-D. Xi, S. Lam, and K.-Q. Xia, “From laminar plumes to organized flows: the onset of
⁴⁴⁵ large-scale circulation in turbulent thermal convection,” *J. Fluid Mech.* **503**, 47–56 (2004).
⁴⁴⁶ ⁴⁷Q. Zhou, C. Sun, and K.-Q. Xia, “Morphological Evolution of Thermal Plumes in Tur-
⁴⁴⁷ bulent Rayleigh-Bénard Convection,” *Phys. Rev. Lett.* **98**, 074501 (2007).
⁴⁴⁸ ⁴⁸C. Sun, Q. Zhou, and K.-Q. Xia, “Cascades of Velocity and Temperature Fluctuations in
⁴⁴⁹ Buoyancy-Driven Turbulence,” *Phys. Rev. Lett.* **97**, 144504 (2006).
⁴⁵⁰ ⁴⁹Q. Zhou, C. Sun, and K.-Q. Xia, “Experimental Investigation of Homogeneity, Isotropy,
⁴⁵¹ and Circulation of the Velocity Field in Buoyancy-Driven Turbulence,” *J. Fluid Mech.*
⁴⁵² **598**, 361–372 (2008).
⁴⁵³ ⁵⁰G.-W. He and J.-B. Zhang, “Elliptic model for space-time correlations in turbulent shear
⁴⁵⁴ flows,” *Phys. Rev. E* **73**, 055303(R) (2006).
⁴⁵⁵ ⁵¹X. Zhao and G.-W. He, “Space-time correlations of fluctuating velocities in turbulent shear
⁴⁵⁶ flows,” *Phys. Rev. E* **79**, 046316 (2009).
⁴⁵⁷ ⁵²X.-Z. He, G.-W. He, and P. Tong, “Small-scale turbulent fluctuations beyond Taylor’s
⁴⁵⁸ frozen-flow hypothesis,” *Phys. Rev. E* **81**, 065303(R) (2010).
⁴⁵⁹ ⁵³X.-Z. He and P. Tong, “Kraichnan’s random sweeping hypothesis in homogeneous turbulent
⁴⁶⁰ convection,” *Phys. Rev. E* **83**, 037302 (2011).
⁴⁶¹ ⁵⁴Q. Zhou, C. Li, Z. Lu, and Y. Liu, “Experimental Investigation of Longitudinal Space-
⁴⁶² Time Correlations of the Velocity Field in Turbulent Rayleigh-Bénard Convection,” *J.*
⁴⁶³ *Fluid Mech.* **683**, 94–111 (2011).
⁴⁶⁴ ⁵⁵S. Grossmann and D. Lohse, “Scaling in thermal convection: a unifying theory,” *J. Fluid*
⁴⁶⁵ *Mech.* **407**, 27–56 (2000).
⁴⁶⁶ ⁵⁶S. Grossmann and D. Lohse, “Thermal convection for large Prandtl numbers,” *Phys. Rev.*
⁴⁶⁷ *Lett.* **86**, 3316–3319 (2001).
⁴⁶⁸ ⁵⁷S. Grossmann and D. Lohse, “Prandtl and Rayleigh number dependence of the Reynolds
⁴⁶⁹ number in turbulent thermal convection,” *Phys. Rev. E* **66**, 016305 (2002).
⁴⁷⁰ ⁵⁸S. Grossmann and D. Lohse, “Fluctuations in turbulent Rayleigh-Bénard convection: the
⁴⁷¹ role of plumes,” *Physics of fluids* **16**, 4462 (2004).
⁴⁷² ⁵⁹R. Ni, S. Huang, and K.-Q. Xia, “Local Energy Dissipation Rate Balances Local Heat Flux
⁴⁷³ in the Center of Turbulent Thermal Convection,” *Phys. Rev. Lett.* **107**, 174503 (2011).